Optical Engineering

OpticalEngineering.SPIEDigitalLibrary.org

# Simple ps microchip Nd:$YVO_4$ laser with 3.3-ps pulses at 0.2 to 1.4 MHz and single-stage amplification to the microjoule level

Erdal Türkyilmaz
Jan Lohbreier
Christian Günther
Eva Mehner
Daniel Kopf
Harald Giessen
Bernd Braun

Erdal Türkyilmaz, Jan Lohbreier, Christian Günther, Eva Mehner, Daniel Kopf, Harald Giessen, Bernd Braun, "Simple ps microchip Nd:$YVO_4$ laser with 3.3-ps pulses at 0.2 to 1.4 MHz and single-stage amplification to the microjoule level," *Opt. Eng.* **55**(6), 066126 (2016), doi: 10.1117/1.OE.55.6.066126.

# Simple ps microchip $Nd:YVO_4$ laser with 3.3-ps pulses at 0.2 to 1.4 MHz and single-stage amplification to the microjoule level

**Erdal Türkyilmaz,[a] Jan Lohbreier,[b] Christian Günther,[b] Eva Mehner,[b] Daniel Kopf,[a] Harald Giessen,[c] and Bernd Braun[b,*]**
[a]Montfort Laser GmbH, Im Holderlob 6a, A-6840 Götzis, Austria
[b]Nuremberg Institute of Technology Georg Simon Ohm, Faculty of Applied Mathematics, Physics and Humanities, Keßlerplatz 12, 90489 Nuremberg, Germany
[c]University of Stuttgart, 4th Physics Institute and Stuttgart Center of Photonics Engineering, Pfaffenwaldring 57, 70550 Stuttgart, Germany

**Abstract.** Commercial picosecond sources have found widespread applications. Typical system parameters are pulse widths below 20 ps, repetition rates between 0.1 and 2 MHz, and microjoule level pulse energies. Most systems are based on short pulse mode-locked oscillators, regenerative amplifiers, and pockel cells as active beam switches. In contrast, we present a completely passive system, consisting of a passively Q-switched microchip laser, a single-stage amplifier, and a pulse compressor. The Q-switched microchip laser has a 50-$\mu$m-long $Nd:YVO_4$ gain material optically bonded to a 4.6-mm-thick undoped $YVO_4$ crystal. It delivers pulse widths of 40 ps and repetition rates of 0.2 to 1.4 MHz at a wavelength of 1.064 $\mu$m. The pulse energy is a few nanojoule. These 40-ps pulses are spectrally broadened in a standard single-mode fiber and then compressed in a 24-mm-long chirped Bragg grating to as low as 3.3 ps. The repetition rate can be tuned from ~0.2 to 1.4 MHz by changing the pump power, while the pulse width and the pulse energy from the microchip laser are unchanged. The spectral broadening in the fiber is observed throughout the pulse repetition rate, supporting sub-10-ps pulses. Finally, the pulses are amplified in a single-stage $Nd:YVO_4$ amplifier up to the microjoule level (up to 4 $\mu$J pulse energy). As a result, the system delivers sub-10-ps pulses at a microjoule level with about 1 MHz repetition rate, and thus fulfills the requirements for ps-micromachining. It does not contain any active switching elements and can be integrated in a very compact setup.  [DOI: 10.1117/1.OE.55.6.066126]

Keywords: microchip laser; picosecond pulsed lasers; short pulses; passively Q-switched; micromachining.

Paper 160181P received Feb. 5, 2016; accepted for publication Jun. 10, 2016; published online Jun. 29, 2016.

## 1 Introduction

Picosecond pulsed laser systems have become a standard tool in micromachining of metals and semiconductors. When the pulse duration is short in comparison to thermal relaxation times, the light energy primarily heats up the electrons and leads to an evaporation of the material before being transferred to the phonon system of the lattice.[1,2] That is why this kind of micromachining is called "cold" material processing. The laser parameters necessary for these applications are as follows: the pulse width should be between 1 and 20 ps, the pulse repetition rate should be tunable between some hundred kHz and a few MHz, and the pulse energy should reach the microjoule level. These system parameters can be realized with four different concepts: either with mode-locked oscillators and regenerative amplifiers, with multipass-cell-oscillators, with cavity-dumped systems, or with amplified passively Q-switched microchip lasers. Mode-locked oscillators in combination with a regenerative amplifier are most commonly used for micromachining, but consist of two resonators and at least one active beam switch. Thus, these systems are complex and expensive. With cavity-dumped systems and multipass-cell-oscillators, the parameters listed above could be demonstrated,[3–5] but these lasers did not find their way to industrial applications due to the length or the complexity of the systems. The advent of passively Q-switched microchip lasers led to a drastic reduction of the Q-switched pulse widths below 1 ns.[6–8] Theoretical investigations show that the pulse width linearly scales with the cavity length.[9–13] Thus with bulk saturable absorbers such as $Cr^{4+}:YAG$,[8] the pulse widths are limited to a few hundred picoseconds. In contrast, if a semiconductor saturable absorber (SESAM[14]) is used as an end mirror, it rarely increases the cavity length (just by the penetration depth of around 1 $\mu$m). With this approach, a major reduction of the pulse width down to 56 ps,[12] 36 ps,[13] and more recently 22 ps[15] and even 16 ps[16] could be demonstrated. Going below a limit of a few ten picoseconds enables a Q-switched laser, for the very first time, to be used as a very compact and simple seed source in an oscillator–amplifier system. If a microchip laser is paired with a succeeding amplifier stage,[17–20] a sufficiently high pulse energy for micromachining applications can be reached. Rather than pushing the limit with respect to the pulse width, an alternative approach has been reported previously.[20,21] It makes use of a microchip laser with moderate pulse width of a few ten picoseconds and subsequent reduction of the pulse width down to a few picoseconds or even femtoseconds by spectral broadening in a

*Address all correspondence to: Bernd Braun, E-mail: bernd.braun@th-nuernberg.de

0091-3286/2016/$25.00 © 2016 SPIE

fiber and subsequent pulse compression. Reference 20 reports amplification of such spectrally broadened pulses in a dual-stage rod fiber-based arrangement with a >1-m form factor, and Ref. 21 describes a pulse shortening setup achieving <200 fs with nJ energies, starting from a ~100-ps microchip laser as the front end.

In this paper, we describe a setup of a Q-switched microchip laser with a pulse width of about 40 ps, a moderate pulse reduction by one order of magnitude to 3 ps, and finally the amplification in a simple, single-stage Nd:YVO$_4$ amplifier to the microjoule energy level suitable for micromachining applications.

## 2 Q-Switched Microchip Laser

The experimental setup is shown in Fig. 1. A fiber-coupled diode laser (Lumics) was used as a pump source with an output power of 2 W, a numerical aperture of 0.12, and a core diameter of 50 $\mu$m. The pump light is imaged with a $f = 13.86$-mm collimation lens and a $f = 4.51$-mm aspheric lens onto the $Nd^{3+}$:YVO$_4$ crystal. Thus, a pump spot diameter of about 25 $\mu$m is achieved. The crystal assembly consists of an undoped YVO$_4$ crystal with a length of ~4.6 mm, which is optically bonded to a 3 at. %-doped $Nd^{3+}$:YVO$_4$ crystal with a thickness of 50 $\mu$m. The bonded crystal structure is the key component to reach short Q-switched pulse widths. First, it enables the handling of an ultrathin crystal plate; second, it allows adjustment to the longitudinal heat flow and thus the resulting thermal lens, which in turn stabilizes the resonator.[16] The interface between the doped and undoped YVO$_4$ crystal is coated with a partial reflectivity of 90% (10% output coupling) for the laser wavelength at 1.064 $\mu$m and with an antireflection coating for the pump wavelength at 808 nm. An SESAM[14] is used as a second end mirror. It has a nominal modulation depth of 5% and nonsaturable losses of about 1% to 2%. The recovery time is on the order of some hundred picoseconds, which results in a low-saturation intensity and a fast bleaching of the absorber. The saturation fluence is estimated to be ~120 $\mu$J/cm$^2$. Finally, the Q-switched output beam is separated from the pump beam by a dichroic beam splitter (DBS).

At a pump power of 1.13 W, a maximum pulsed output power of 28 mW and a repetition rate of 1.1 MHz are achieved, resulting in a pulse energy of 30 nJ. The pulse width is 40 ps, measured with a long-scan autocorrelator and assuming a sech$^2$-pulse shape. By changing the pump power from 0.27 to 1.13 W, the repetition rate can be tuned from 0.2 MHz to above 1 MHz, while the pulse width and the pulse energy stay constant as is to be expected by theory. The beam quality was measured to be $M^2 = 1.35$ up to a pump power of 1.13 W.

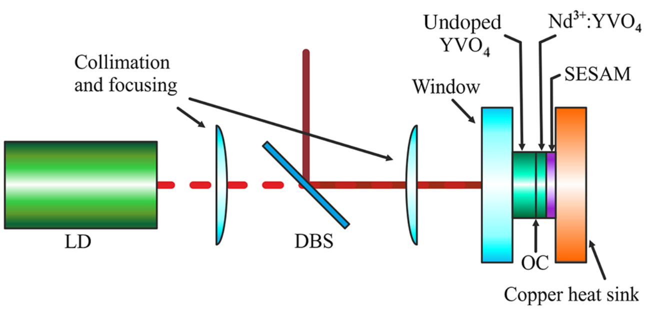


**Fig. 1** Schematic design of the experimental setup: passively Q-switched microchip laser pumped by an LD with output coupler (OC) and a DBS for separation of pump and laser radiation.

## 3 Finite Element Method-Simulations

For two reasons, the finite element method (FEM) was employed to analyze the microchip laser. First, the laser resonator without a thermal lens acts like a Fabry–Perot flat–flat resonator and thus is metastable. A convex thermal lens is needed to stabilize the resonator. The focal length of this thermal lens needs to be adjusted in such a way that the resulting laser mode matches the pump mode to guarantee a diffraction limited beam quality.[22] This in turn is essential to obtain a stable pulse train with low-frequency jitter because otherwise mode beating and mode competition would result in severe amplitude and frequency fluctuations.

Second, the power density within the focal volume is some tens of nW/cm$^3$. The corresponding heat input into the material causes an inhomogeneous temperature distribution, ultimately giving rise to thermal lensing. Also, this temperature field generates tensile and compressive stresses within the crystal. Therefore, the long-term mechanical stability of the optical bonds as well as the bulk material is an issue.

To simulate the consequences of the heat deposited within the focal spot, an FEM-simulation was conducted. As a software, the commercially available COMSOL Multiphysics was used, including the packages for heat transfer and structural mechanics. Utilizing a fully coupled algorithm, the temperature distribution as well as the resulting stresses and strains is computed parallel.

One challenge of this model is the scaling: on one hand, the overall crystal with about 1-mm edge length and on the other hand, the micrometer-sized focal spot. Since the dimensions differ by more than two orders of magnitude, a structured mesh with a mesh gradient was employed. This way, the necessary resolution is achievable, while the computing time is still acceptable. For reasons of simplification, the two optical coatings are approximated as two-dimensional thin objects with a defined heat resistance and no physical thickness.

The temperature of the copper heat sink at the front face and the temperature at the rear face of the undoped crystal were assumed to be constant at 23°C. At the lateral surface of the crystal, the gradient of the temperature profile was assumed to be constant. Thus, no heat transfer is allowed via the lateral surface to the surrounding air. The basic modeling parameters are $l_{\mathrm{Nd:YVO}} = 50\ \mu\mathrm{m}$, $l_{\mathrm{YVO}} = 1$ mm, $l_{\mathrm{GaAs}} = 650\ \mu\mathrm{m}$, $2w_{\mathrm{pump}} = 25\ \mu\mathrm{m}$, and $P_{\mathrm{heat}} = 25$ mW. The fixed point for the mechanical stresses is the GaAs side facing the copper heat sink.

### 3.1 *Temperature*

In Figs. 2 and 3, the temperature distribution within the crystal is shown. As can be seen in Fig. 2, the maximum temperature—about 320 K—is located within the focal spot closer to the YVO$_4$ (left) side. This is due to the significantly better heat transfer through GaAs on the right-hand side.

In Fig. 3, one can clearly see the difference in heat conduction between the YVO$_4$ and GaAs side. Having a roughly ten times higher thermal conductivity than YVO$_4$, GaAs

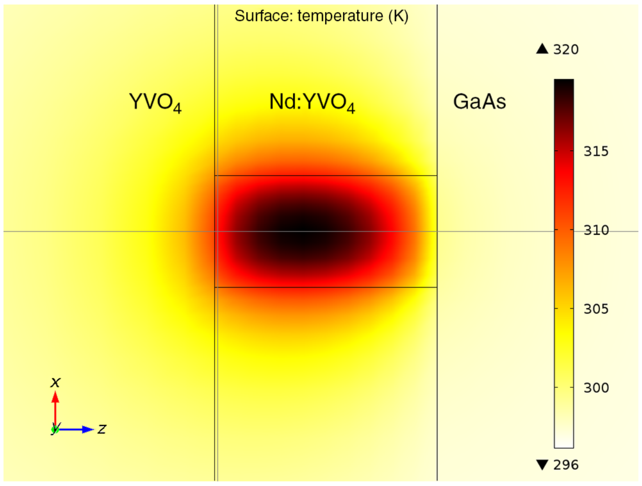


**Fig. 2** Temperature distribution on the $x-z$ plane, which goes through the optical axis ($y = 0$). The darker the color, the higher the temperature. The black contoured rectangle in the middle matches the focal spot. The temperature distribution in the $y-z$ plane (not displayed here) is similar.

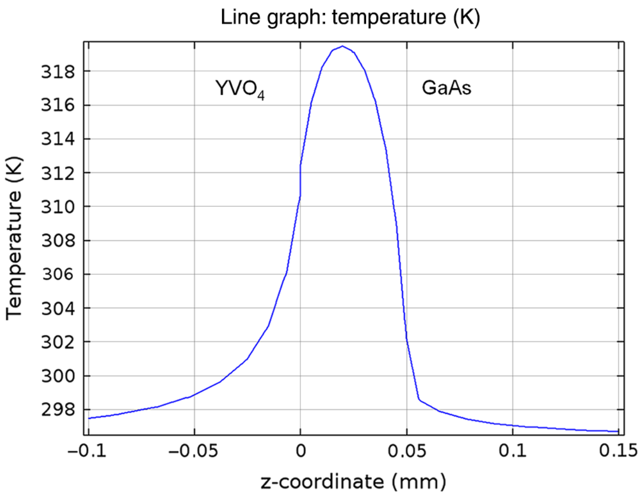


**Fig. 3** Temperature distribution along the $z$-axis (optical axis, $x = y = 0$). The maximum is at about $z = 0.02$ mm, a little closer to the YVO end than to the GaAs end. From this maximum, there is a decrease in the temperature toward both sides. The gradient toward GaAs is much higher than toward YVO.

transports the heat much more effectively toward the cool end wall. As mentioned in the capture, this leads to a steeper decline of the temperature on the right side and thus a higher temperature gradient.

By fitting the radial heat distribution at different longitudinal positions (not shown here), a parabolic function of the refractive index can be deduced from the parabolic temperature profile. This corresponds to a sequence of Gaussian ducts, which can be approximated by a single thermal lens. For the above noted parameters, a value of $f = 35$ mm is computed.

### 3.2 *Stresses*

By heating up the focal spot, the crystal expands and since it consists of three materials with differing, and partly anisotropic, moduli of elasticity and thermal expansion coefficients, a rather complex deformation takes place. This is shown qualitatively in Fig. 4. The stress used here is the von Mises stress, which can be interpreted as the scalar stress value of the Cauchy stress tensor. It serves as a value for analytical understanding and to anticipate potential stability issues of the laser crystal.

As it is indicated in Fig. 4, the deformation along the $y$- and $x$-axis is not identical. This can be attributed to the anisotropic modulus of elasticity of (Nd:)YVO$_4$. In Figs. 5(a) and 5(b), the stress distribution within the crystal is shown along these two planes to find the potentially critical locations. In detail, the spots with the highest stress are:

- The global maximum stress is found at the highest temperature gradient between the doped Nd:YVO$_4$ and the GaAs. At this point, it reaches up to about 23.1 MPa and is a tensile stress.
- A second local maximum lies inside the crystal. This compressive stress is due to the maximum temperature and the resulting maximum thermal expansion. It reaches about 80% of the global maximum stress.
- A third location with a noticeable increase in stress is radially outside the focal spot. This only appears on Fig. 5(b) and stems from a high-temperature gradient in the $x$-direction leading to tensile stress. It peaks around 16 MPa.

## 4 Amplification and Pulse Compression

The experimental setup of the single-stage amplification and the compressor is shown in Fig. 6. The output from the microchip laser is spectrally broadened in a 50-m-long standard single-mode fiber (HI1060, 125 $\mu$m Cladding). The spectral bandwidth after the fiber is broadened by one order of magnitude to 0.42-nm FWHM with the center wavelength at 1064.2 nm. In Fig. 7(a), the optical spectrum after the pulse propagation through the 50-m fiber is shown. It was measured with the optical spectrum analyzer AQ6317B by ANDO with a resolution bandwidth of 0.02 nm.

The pulses are amplified in a single-stage Nd:YVO$_4$ amplifier with a 11-mm-long Nd:YVO$_4$ crystal, pumped by a fiber-coupled Lissotschenko Mikrooptik GmbH laser diode (LD). The diode delivers up to 32 W optical power at a wavelength of 880 nm. The core diameter is about 200 $\mu$m and the numerical aperture is 0.22. The pump radiation is collimated ($f = 40$ mm) and focused ($f = 60$ mm) by a pair of aspheric lenses. After double-pass through the crystal the Faraday rotator was used for separating input and output pulses and an amplified pulse energy of more than 4 $\mu$J could be reached. Finally, the pulses are then compressed in a 24-mm long chirped Bragg grating (CBG) from Optigrate, Inc. to as low as 3.3 ps. The CBG has a linear group delay dispersion of ~54.5 ps/nm, a spectral bandwidth of 4.1 nm, and a grating period of about 360 nm. After the CBG, the pulse width was measured with an autocorrelator, assuming a sech$^2$-pulse shape [Fig. 7(b)]. The pulse duration was measured with a "pulseCheckUSB" autocorrelator by APE Angewandte Physik und Elektronik GmbH, Berlin.

The pump power of the fiber-coupled LD was varied at a constant repetition rate. Both the amplified power and the

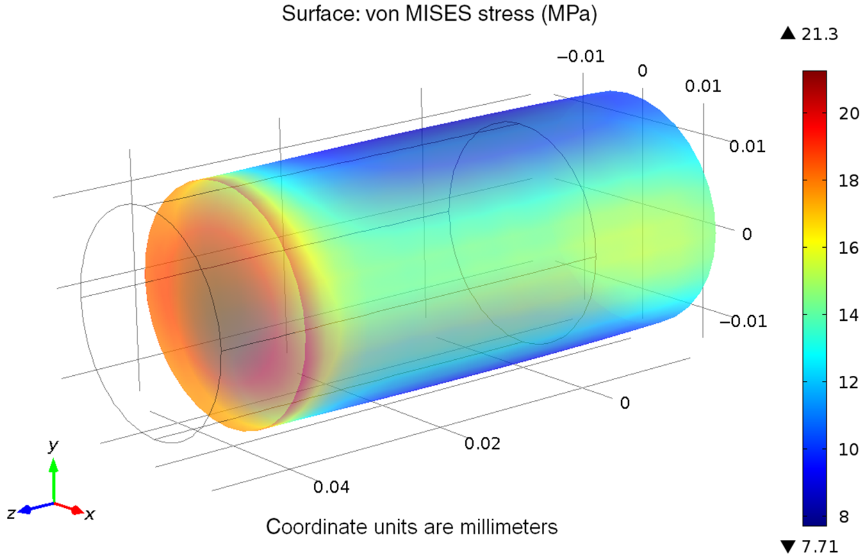


**Fig. 4** Displayed is only the focal spot volume, in which the energy of the pump laser is deposited. On the surface of this originally cylindrical shape (black contour in background), the stresses in MPa can be seen. The perspective is from the GaAs and toward the YVO$_4$ end. For clarification, the displacement is scaled up by a factor of 1000. The absolute movement in the negative $z$-direction can be explained by the fixed GaAs surface toward the heat sink and thermal expansion of the complete crystal.

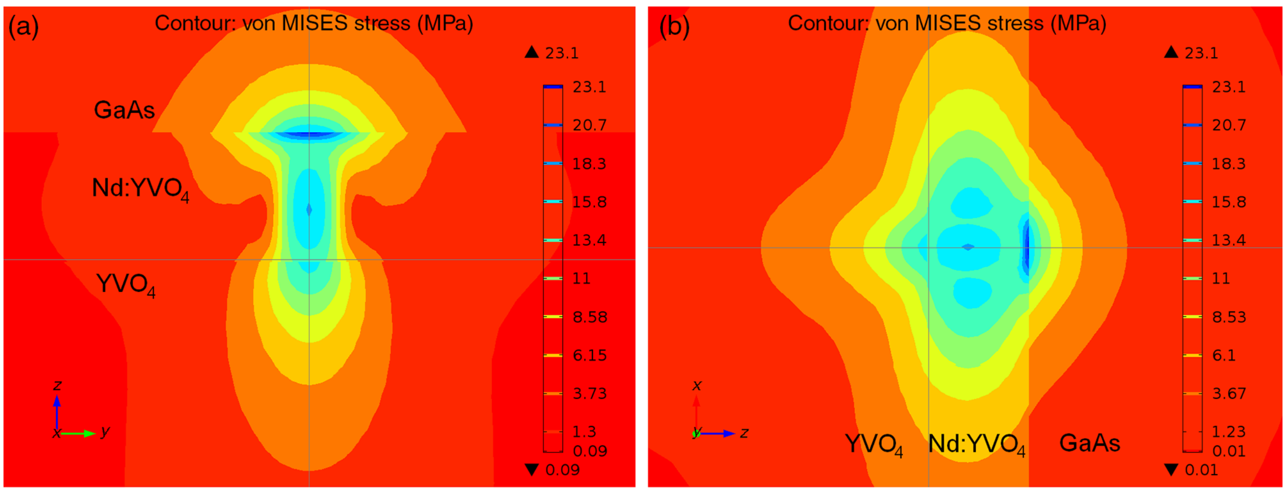


**Fig. 5** The stress distribution is shown in two dimensions: (a) depicts the $y-z$ plane and (b) depicts the $x-z$ plane. The color legend is nearly identical and shows the von Mises stress in and around the focal spot region (thickness of the Nd:YVO$_4$ layer is 50 $\mu$m).

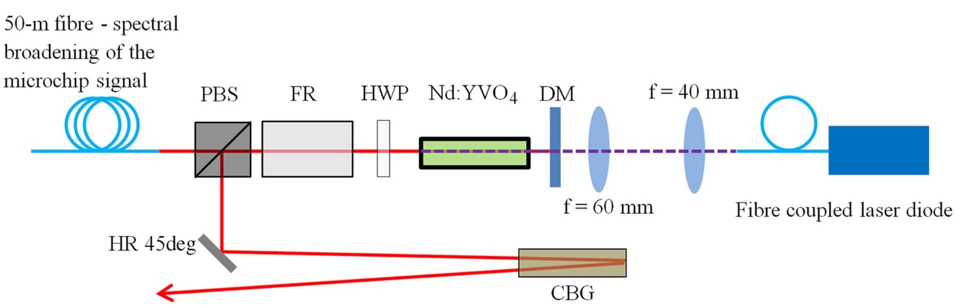


**Fig. 6** Schematic of the single-stage amplification and the pulse compressor. PBS, polarizing beam splitter; FR, Faraday rotator; HWP, half-waveplate; DM, dichroic mirror; and CBG, chirped Bragg grating.

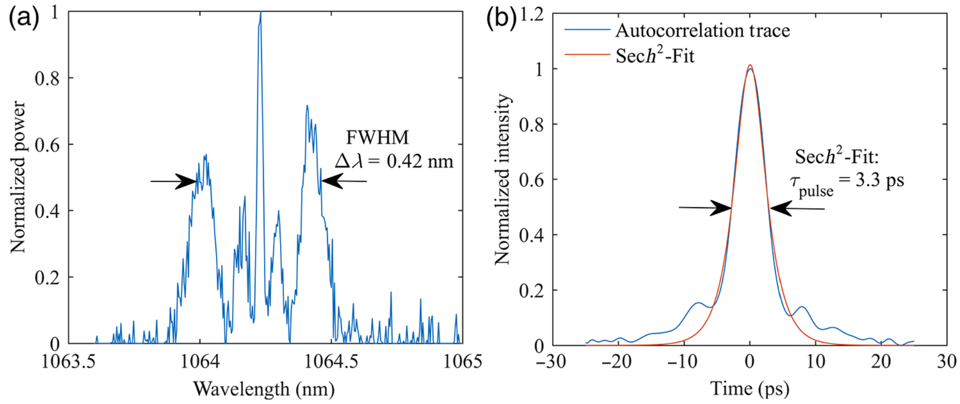


**Fig. 7** (a) Optical spectrum of a Q-switched pulse measured direct after pulse propagation through the 50-m fiber and (b) autocorrelation trace measured after the CBG without amplification, fitted by a sech$^2$-function.

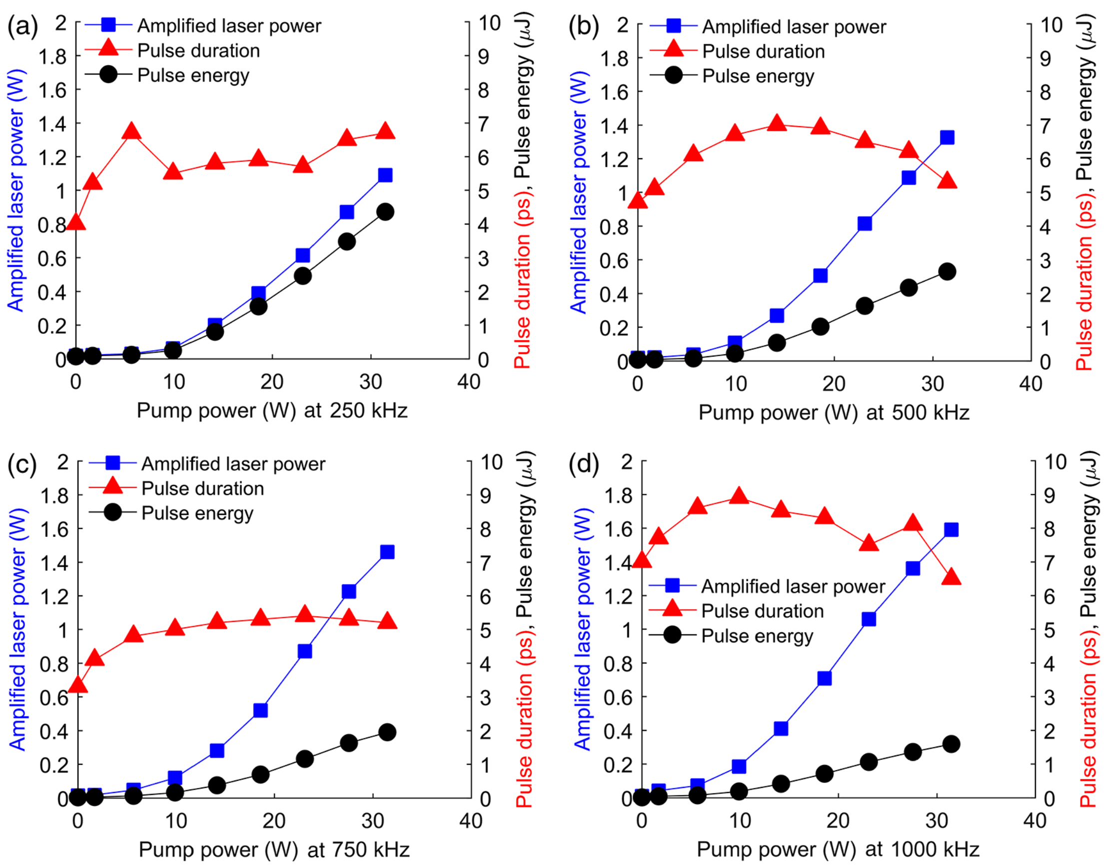


**Fig. 8** Average laser power (squares), pulse width (triangles), and pulse energies (circles) as a function of pump power at (a) 250 kHz, (b) 500 kHz, (c) 750 kHz, and (d) 1 MHz repetition rate.

pulse energy rise linearly as a function of the pump power and the pulse width stays nearly constant (Fig. 8).

## 5 Conclusion

We have demonstrated a simple laser system consisting of a passively Q-switched microchip laser, a single-stage amplifier and pulse compressor. The laser delivers 3-ps pulses at a repetition rate of about 1 MHz with a pulse energy of some $\mu$J. By changing the pump power of the microchip, it is possible to adjust the repetition rate from 0.2 to 1.4 MHz, while the pulse width and the pulse energy stay constant. FEM-simulations are key to understanding the thermal properties and the mechanical stresses of the setup. According to Refs. 23 and 24, the known thermal fracture limit of $YVO_4$ is ~50 MPa, which means ours system operates at less than half the critical level. The laser system does not contain any active switching components and can be integrated in a very compact setup.

### *References*

1. B. N. Chichkov et al., "Femtosecond, picosecond and nanosecond laser ablation of solids," *Appl. Phys. A* **63**, 109–115 (1996).

2. R. Le Harzic et al., "Pulse width and energy influence on laser micromachining of metals in a range of 100 fs to 5 ps," *Appl. Surf. Sci.* **249**, 322–331 (2005).
3. A. Killi et al., "High-peak-power pulses from a cavity-dumped Yb:KY(WO$_4$)$_2$ oscillator," *Opt. Lett.* **30**, 1891–1893 (2005).
4. V. Z. Kolev et al., "Passive mode locking of a Nd:YVO$_4$ laser with an extra-long optical resonator," *Opt. Lett.* **28**, 1275–1277 (2003).
5. D. N. Papadopoulos et al., "Passively mode-locked diode-pumped Nd:YVO$_4$ oscillator operating at an ultralow repetition rate," *Opt. Lett.* **28**, 1838–1841 (2003).
6. J. J. Zayhowski, "Q-switched operation of microchip lasers," *Opt. Lett.* **16**, 575–577 (1991).
7. J. J. Zayhowski, "Microchip lasers," *Opt. Mater.* **11**, 255–267 (1999).
8. J. J. Zayhowski and C. Dill, "Diode-pumped passively Q-switched picosecond microchip lasers," *Opt. Lett.* **19**, 1427–1429 (1994).
9. J. J. Zayhowski and P. L. Kelly, "Optimization of Q-switched lasers," *IEEE J. Quantum Electron.* **27**, 2220–2225 (1991).
10. J. J. Zayhowski and P. L. Kelly, "Correction to "optimization of Q-switched lasers," *IEEE J. Quantum Electron.* **29**, 1239 (1993).
11. J. J. Degnan "Optimization of passively Q-switched lasers," *IEEE J. Quantum Electron.* **31**, 1890–1901 (1995).
12. B. Braun et al., "56-ps passively Q-switched diode-pumped microchip laser," *Opt. Lett.* **22**, 381–383 (1997).
13. G. J. Spühler et al., "Experimentally confirmed design guidelines for passively Q-switched microchip lasers using semiconductor saturable absorbers," *J. Opt. Soc. Am. B* **16**, 376 (1999).
14. U. Keller et al., "Semiconductor saturable absorber mirrors (SESAM's) for femtosecond to nanosecond pulse generation in solid-state lasers," *IEEE J. Sel. Top. Quantum Electron.* **2**, 435–453 (1996).
15. A. C. Butler, D. J. Spence, and D. W. Coutts, "Scaling Q-switched microchip lasers for shortest pulses," *Appl. Phys. B* **109**, 81–88 (2012).
16. E. Mehner et al., "Sub-20 ps pulses from a passively Q-switched microchip laser at 1 MHz repetition rate," *Opt. Lett.* **39**, 2940–2943 (2014).
17. C. D. Brooks and F. Di Teodoro, "Multimegawatt peak-power, single-transverse-mode operation of a 100 $\mu$m core diameter, Yb-doped rod-like photonic crystal fiber amplifier," *Appl. Phys. Lett.* **89**, 111119 (2006).
18. D. Nodop et al., "High-pulse-energy passively Q-switched quasi-monolithic microchip lasers operating in the sub- 100-ps pulse regime," *Opt. Lett.* **32**, 2115–2117 (2007).
19. O. Schmidt et al., "105 kHz, 85 ps, 3 MW peak power microchip laser fiber amplifier system," in *Advanced Solid-State Photonics*, paper WB23, Optical Society of America (2008).
20. A. Steinmetz et al., "Sub-5-ps, multimegawatt peak-power pulses from a fiber-amplified and optically compressed passively Q-switched microchip laser," *Opt. Lett.* **37**, 2550–2552 (2012).
21. R. Lehneis et al., "All-fiber pulse shortening of passively Q-switched microchip laser pulses down to sub-200 fs," *Opt. Lett.* **39**, 5806–5809 (2014).
22. E. Mehner et al., "Stable MHz-repetition-rate passively Q-switched microchip laser frequency doubled by MgO:PPLN," *Appl. Phys. B* **112**, 231–239 (2013).
23. Y. F. Chen, "Influence of thermal fracture on scaling diode end-pumped laser to high power," in *Conference on Lasers and Electro-Optics (CLEO)*, paper CTuK28, 128 (1999).
24. D. Krennrich, "Erzeugung und Charakterisierung Ultrakurzer Lichtimpulse von Diodengepumpten Modengekoppelten Festkörperlasern mit Neodym Dotierten Lasermaterialien im Wellenlängenbereich von 0, 9 $\mu$m bis 1, 3 $\mu$m," Cuvillier Verlag, Göttingen (2005).

**Erdal Türkyilmaz** received his diploma in physics and mathematics from the University of Innsbruck in 2013. Currently, he is a laser physicist and project leader for ultrafast lasers at Montfort Laser GmbH in Götzis. Since 2014, he has also taught physics in the Higher Technical Institute of Rankweil.

**Jan Lohbreier** received his doctoral degree in physics at the University of Würzburg, Germany, in 2008. In the field of laser physics, he worked on the generation and control of high-order harmonics in the extreme ultraviolet regime regime. After this, he was working for several years in the Engineering Departments of Robert Bosch GmbH. In 2014, he accepted an appointment as professor in physics at Nuremberg Institute of Technology. In addition to teaching general physics, his field of research is numerical simulation of multiphysical phenomena.

**Christian Günther** studied physics at the University of Leipzig with a strong focus on experimental physics, particularly solid-state physics. His diploma thesis on the observation of phase formations by *in situ* x-ray diffraction observations observations was done in collaboration with the Leibniz-Institut für Oberflächenmodifizierung e.V. in Leipzig. After his studies, he worked at the University of Applied Science in Nuremberg (Technische Hochschule Nürnberg), developing innovative new laser sources and doing research on laser solid interaction.

**Eva Mehner** studied laser technologies and optotechnologies at the University of Applied Sciences in Jena, Germany. She received her BE degree in 2006 and her ME degree in 2009. In her theses at Jenoptik and Trumpf, her main focus was on regenerative amplifiers. Since 2009, her research interests have been michrochip lasers and the generation of short pulses at the University of Applied Sciences in Nuremberg.

**Daniel Kopf** studied physics and wrote his PhD thesis at ETH Zurich, Switzerland, on compact diode-pumped solid-state lasers. He founded High Q Laser GmbH in 1999 to commercialize femtosecond lasers (now part of Newport, Spectra Physics). Since 2012, he is founder and CEO of Montfort Laser GmbH, Austria, a company that develops compact pulsed solid-state lasers. His main research interests are microchip picosecond lasers, femtosecond lasers, compact Nd:YAG lasers, and optical coatings.

**Harald Giessen** is a full professor and holds the Chair for Ultrafast Nanooptics in the Department of Physics at the University of Stuttgart. He is also the cochair of the Stuttgart Center of Photonics Engineering. His research interests include ultrafast nanooptics, plasmonics, metamaterials, three-dimensional printed micro and nanooptics, novel mid-IR ultrafast laser sources, and applications in microscopy, biology, and sensing. He received an European Research Council Advanced Grant in 2012 for his work on complex nanoplasmonics.

**Bernd Braun** received his PhD degree in physics from the Swiss Federal Institute of Technology in Zurich (ETH Zürich). For nearly 10 years, he has worked for industrial companies in the field of optical coatings and mode-locked oscillators. Since 2005, he has been a professor of physics at the University of Applied Science in Nuremberg (Technische Hochschule Nürnberg). He teaches applied physics, laser physics, quantum physics, and technical optics. His research interests include compact, short-pulse laser sources, and their applications in micromachining.